

Temporal comparison of functional brain imaging with diffuse optical tomography and fMRI during rat forepaw stimulation

Andrew M Siegel¹, Joseph P Culver², Joseph B Mandeville²
and David A Boas²

¹ Tufts University Bioengineering Center, Medford, MA 02155, USA

² Martinos Center for Biomedical Imaging, Massachusetts General Hospital,
Harvard Medical School, Boston, MA 02129, USA

E-mail: siegel@ll.mit.edu

Received 8 January 2003

Published 7 May 2003

Online at stacks.iop.org/PMB/48/1391

Abstract

The time courses of oxyhaemoglobin ([HbO₂]), deoxyhaemoglobin ([HbR]) and total haemoglobin ([HbT]) concentration changes following cortical activation in rats by electrical forepaw stimulation were measured using diffuse optical tomography (DOT) and compared to similar measurements performed previously with fMRI at 2.0 T and 4.7 T. We also explored the qualitative effects of varying stimulus parameters on the temporal evolution of the hemodynamic response. DOT images were reconstructed at a depth of 1.5 mm over a 1 cm square area from 2 mm anterior to bregma to 8 mm posterior to bregma. The measurement set included 9 sources and 16 detectors with an imaging frame rate of 10 Hz. Both DOT [HbR] and [HbO₂] time courses were compared to the fMRI BOLD time course during stimulation, and the DOT [HbT] time course was compared to the fMRI cerebral plasma volume (CPV) time course. We believe that DOT and fMRI can provide similar temporal information for both blood volume and deoxyhaemoglobin changes, which helps to cross-validate these two techniques and to demonstrate that DOT can be useful as a complementary modality to fMRI for investigating the hemodynamic response to neuronal activity.

(Some figures in this article are in colour only in the electronic version)

1. Introduction

Functional magnetic resonance imaging (fMRI) has led to significant advances in neuroimaging during the last 10 years (Habel *et al* 2002, Dale and Halgren 2001, Berns 1999). It allows near real-time observation of the hemodynamic response to neuronal activation.

The BOLD fMRI signal scales approximately with absolute changes in deoxyhaemoglobin ([HbR]); however, questions remain about the exact relationship between the BOLD signal and the vascular response. Likewise the coupling between neural activity and the vascular response itself is poorly understood (Villringer and Dirnagl 1995, Arthurs *et al* 2000). Since MRI and diffuse optical tomography (DOT) are based upon different fundamental principles, cross-validation can help us to better understand both the neurophysiology behind cortical activation and the biophysics behind the measurement techniques themselves.

In this paper, we compare fMRI and DOT measurements of the temporal evolution of the hemodynamic response to electrical forepaw stimulation in rat somatosensory cortex. DOT is a noninvasive neuroimaging technique which exploits both the spectrally varying absorption and diffuse scattering nature of near-infrared light propagation through tissue (Boas *et al* 2001, Hintz *et al* 2001, Villringer and Chance 1997). Unlike fMRI, DOT can directly and simultaneously measure concentration changes in deoxyhaemoglobin ([HbR]), oxyhaemoglobin ([HbO₂]) and total haemoglobin ([HbT] = [HbR] + [HbO₂]) in cortical tissue.

We set out to cross-validate this new technique with fMRI. Other researchers have observed qualitative spatial (Benaron *et al* 2000, Kleinschmidt *et al* 1996, Strangman *et al* 2002) and temporal (Toronov *et al* 2001) correspondence between the fMRI BOLD signal and diffuse optical measures of [Hb] and [HbO₂] in humans; however, to date there has been no quantitative examination of the temporal correlation between fMRI and DOT. Previous measurements of rat somatosensory cortex have revealed much about the time course and spatial extent of CBV and BOLD signal following median nerve stimulation in a rodent model (Mandeville *et al* 1999a, Mandeville and Marota 1999, Marota *et al* 1999, Gyngell *et al* 1996, Mandeville *et al* 1998, Ances *et al* 2001). Since this preparation has been well characterized with fMRI, we chose it as a convenient model to cross-validate fMRI and DOT. We also sought to explore the effects of stimulus repetition rate, duration and magnitude, both to determine the robustness of this preparation and to explore the physiology underlying the neurovascular response.

2. Materials and methods

2.1. Anaesthesia

Male Harlan Sprague-Dawley rats of weight 300–400 g were anaesthetized with ~1.8% isoflurane vapour in oxygen enriched (60–80% O₂) air. A core temperature of 36.7 ± 0.5 °C was maintained during the course of the experiment using a laminar heater (Watlow Corp) placed under the ribcage and upper abdomen. The rat was tracheotomized and mechanically ventilated with a custom-designed ventilator using patient-triggered inspiration protected by a time-triggered backup. The ventilator was pressure-cycled, with a peak inspiratory pressure (Paw + tubing drop) of 15 cm H₂O and an inspiratory trigger threshold of between –2 and –5 cm H₂O, which was adjusted as needed to maintain a nominal end-tidal CO₂ of 38 ± 5 Torr. Both were adjusted as needed to maintain adequate ventilation during the experiment. The nominal respiration rate was around 40 BPM. Following tracheotomy, both venous and arterial catheters, each consisting of a 12'' length of PE-10 tubing secured to a luer hub, were placed into the right femoral vessels. After catheterization, a loading dose of 50 mg kg⁻¹ of α -chloralose in saline was administered followed by a continuous venous infusion of between 30 and 45 mg kg⁻¹ h⁻¹, titrated to stabilize the MAP at 100 ± 10 mmHg. The MAP was monitored through the arterial line using a piezoresistive strain gauge sensor (Utah Medical 'Deltran' series). The isoflurane concentration was then reduced to ~0.4% to provide some residual analgesia, during which time the rat was placed in a stereotactic headframe and the optode

assembly was lowered onto the scalp. Once this had been achieved, the isoflurane was discontinued and the stimulator and ECG monitor electrodes were inserted. Our trials began after a 1 h washout period on α -chloralose alone to eliminate any residual hemodynamic effects from the isoflurane. During this time the infusion rate was adjusted to maintain a nominal MAP of 100 mm.

2.2. Biomonitoring

The isoflurane, oxygen and end-tidal CO₂ concentration were measured with a Datex Capnomac anaesthesia monitor. A passive accumulator within the expiratory limb of the ventilator compensated for the small (~3–5 ml) tidal volumes. The accumulator consisted of a tee fitting in series with the Capnomac sampling line to which the empty barrel of a 3 cc syringe was attached. This provided no additional obstruction or backpressure yet offered up to 3 ml of storage volume in which the exhaled breath could accumulate prior to sampling.

The ECG signal was recorded through electrodes fashioned from standard 27 gauge tuberculin needles, cleaned with isopropanol to remove the silicone lubricant normally applied by the manufacturer to reduce the discomfort of needle entry. The two sensing needles were then inserted through skin folds above each shoulder blade, and contact to the ECG preamplifier was made using alligator clips clamped near the protruding end of the needle. A ground needle was inserted along the midline about 1 cm rostral of the tail. The luer hub prevented the needles from exiting the skin. Clean ECG signals with a clearly discernable QRS interval were obtained. The mean arterial pressure was monitored using a commercial piezoresistive blood pressure transducer (Utah Medical Deltran series) operated in direct current mode. The amplifier gain was calibrated to provide a 1V output with a static water column of 136 cm (equivalent to 100 mmHg).

2.3. Stimulation

All stimulation was controlled by a PC computer through a digital IO card, which drove a custom-built stimulus isolation unit equipped with a current delivery monitor. Twenty-seven gauge hypodermic needles, prepared as discussed above, served as stimulus electrodes. The stimulator produced an inductively coupled signal which provided galvanic isolation to minimize electrode polarization. Prior measurements with this stimulator delivering 200 μ s pulses at currents below ~2 mA have shown that the electrode-tissue interface remained stable, with current drift below 5% over an 8 h period. Our pulsewidths were fixed at 200 μ s and the stimulus current ranged from 500 μ A to 2 mA. The temporal data shown here were collected using two stimulus paradigms, both with 2 mA stimulus pulses at a rate of 3 Hz:

- (1) A 6 s stimulus duration (18 pulses) followed by a 54 s recovery period.
- (2) A 30 s stimulus duration (90 pulses) followed by a 90 s recovery period.

The stimulus paradigms used in this study were chosen to mirror those used in the fMRI time course measurements. The short stimulus duration (6 s) was originally selected to provide just enough time for the BOLD response to reach a maximum value, in order to enable the large amount of averaging necessary to investigate small potential transient features such as the BOLD 'initial dip' (Marota *et al* 1999). The longer stimulus duration (30 s) was selected to enable the CPV response to almost reach a maximal response, while avoiding the progressive attenuation that is seen for stimuli of longer durations (Silva *et al* 1999). Delivery was confirmed with a dynamic current monitor circuit, which permitted real-time observation of the current delivered for each stimulus pulse in the train.

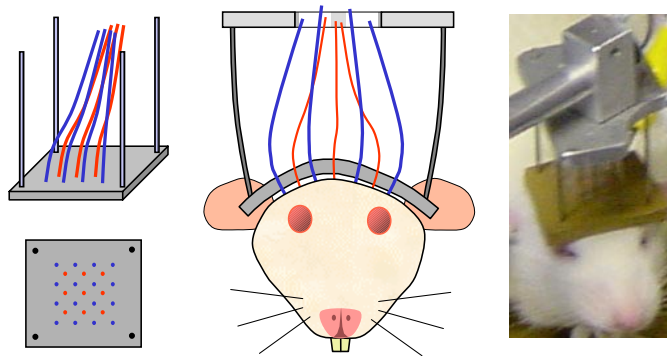


Figure 1. A sketch of the transcutaneous cortical optode assembly and a photo showing its placement. The 3×3 array of source fibres nested within the 4×4 array of detector fibres. Both the rubber pad and steel support tubing flexed, allowing individual optodes to remain normal to the surface while the entire assembly conformed to the curvature of the scalp.

2.4. DOT instrumentation

We used a ‘continuous-wave’ diffuse optical tomography system with an optode assembly consisting of 9 pairs of collocated dual-wavelength (690 nm and 830 nm) fibre-coupled laser diode sources and 16 fibre-coupled silicon APD detectors. Each source was square-wave amplitude-modulated at a single frequency between 4 kHz and 8 kHz with a frequency spacing of 200 Hz. The outputs from each of the 16 APD detector modules were AC-coupled and amplified as needed before being sampled by a 16 bit ADC at a rate of about 40 ksps. The resulting data files were stored on an 80 GB hard disk drive for post-processing.

A diagram of the optode assembly is shown in figure 1. All of the sources and detectors were coupled through 200 μm polymer-clad silica fibre (3M FT-200-URT) to a $1'' \times 1'' \times 0.125''$ thick pliable rubber pad through which the 9 pairs of source fibres and the 16 detector fibres were inserted in a standard ‘9 within 16’ interlaced grid pattern. The row and column spacing was fixed at 0.2'' using a piece of G-10 perfboard as a template to mark the fibre insertion points. This yielded a minimum source-detector spacing of 0.14'' (3.6 mm) and a total grid size of about 0.6'' (15 mm) square. This source-detector spacing was large enough to provide an adequate spatial reconstruction using the methods described below (Kienle and Patterson 1997). The optode pad was anchored at its four corners and suspended about 1.5'' below an aluminium support plate using flexible steel tubing. This design offered a significant degree of compliance which kept the fibre ends normal while allowing the pad and steel tubing to flex to follow the contours of the skull.

2.5. Data processing and image reconstruction

Our raw datafiles were acquired continuously, and consisted of consecutively digitized voltage samples from each of the 16 detector channels at a cyclic collection rate of about 40 ksps for a period of 8 min. This yielded a two-dimensional array of dimension 16 (detectors) \times n (time points), where n was around 19.2 million for an 8 min collection. The first processing step was to bandpass filter the data using a sharp multipole filter algorithm to extract the individual source signals while minimizing the adjacent channel crosstalk. The result of this step was a much smaller 3D array of dimension 16 (detectors) \times 18 (sources) \times m (time points), where

m was now only 4.8 k (10 frames s^{-1} over 8 min). These files were further down sampled to 2 frames s^{-1} with a 1 s time constant low pass filter.

Each 8 min datafile consisted of either four or eight identical trials. The trials within each datafile were then block averaged to reduce the impact of biogenic noise, using the stimulus onset time of each trial for synchronization. The short (~ 15 s) prestimulus period was used to establish an absorbance baseline.

During these experiments, the mechanical ventilator was patient-triggered. The natural variability of patient-triggered ventilation (as opposed to the fixed cycle rate of time-triggered ventilation) led to a greater decorrelation of, and hence more immunity to, the hemomodulating effects of both heartbeat and respiration.

Our voxelation region for image reconstruction consisted of a 40×40 pixel two-dimensional slice, which corresponded to a 2.8×2.8 cm area at a depth of 2.8 mm, from which the actual imagery only represented the central 1.4×1.4 cm portion of this region.

For image reconstructions of spatially varying optical properties, we employed a standard linear approach known as the Rytov approximation, $\Phi = \Phi_0 \exp(\Phi_{\text{scat}})$ (Boas *et al* 2002). The total fluence Φ consists of a background field, Φ_0 , that depends on background optical properties, and a perturbed field, Φ_{scat} , which is linearly related to a set of spatial variations in the optical absorption coefficient $\delta\mu_a$. We discretized the integral into cubic voxels (h^3) and wrote the Rytov approximation as $\mathbf{y} = \mathbf{A}\mathbf{x}$ by making the following associations:

$$y_i = \ln \left[\frac{\Phi(\mathbf{r}_{s,i}, \mathbf{r}_{d,i})}{\Phi_0(\mathbf{r}_{s,i}, \mathbf{r}_{d,i})} \right] \quad A_{i,j} = -\frac{vh^3}{D_0} \frac{G(\mathbf{r}_{s,i}, \mathbf{r}_j)G(\mathbf{r}_j, \mathbf{r}_{d,i})}{G(\mathbf{r}_{s,i}, \mathbf{r}_{d,i})} \quad \text{and} \quad x_j = \delta\mu_{a,j}$$

Here, \mathbf{r}_s and \mathbf{r}_d are the position of the source and detector, respectively; G is the Green's function of the photon diffusion equation for given background optical properties, and a semi-infinite geometry with extrapolated zero boundary conditions. The subscripts i and j represent the indices of each source-detector pair and the indices of each voxel, respectively. The inverse problem was then solved using the (Tikhonov regularized) Moore–Penrose generalized inverse, $\mathbf{x} = \mathbf{A}^T(\mathbf{A}\mathbf{A}^T + \lambda I)^{-1}\mathbf{y}_{\text{meas}}$, where I is the identity matrix (Arridge 1999). We then use a spectroscopic analysis at each voxel to calculate the corresponding $[\text{HbO}_2]$ and $[\text{HbR}]$ changes (Cope and Delpy 1988, Cope 1991).

The activation volume, as measured with fMRI, was approximately 2 mm FWHM (Mandeville and Marota 1999). The spatial resolution of the fMRI measurements was approximately 0.6 mm^3 , and the fMRI data were integrated within a 3 mm^3 sample volume for the time course calculation. For DOT, the voxel size was 0.7 mm^3 and the optical point spread function in the lateral dimension was approximately 2.8 mm^2 , with a constrained vertical depth of 1.4 mm centred at a depth of 2.1 mm. Since our voxel spacing met the Nyquist criterion, the optical point spread function limited the spatial resolution of our imagery, and thus defined the sample volume for our time course calculations. The value of λ , (regularization constant), was chosen to provide a balance between image noise and resolution, as determined by evaluating the contrast to noise ratio (Culver *et al* 2002). This value was kept fixed across all rats, and corresponded to a PSF at the image centre with a FWHM of 2.8 mm (Gaudette 2000, Hansen 1998).

3. Results

A typical spatially resolved image for a single rat is shown in figure 2. Based upon such spatial maps, the individual DOT time courses were extracted from the region of maximal activation, elicited by electrical forepaw stimulation using the 6 and 30 s stimulus paradigms described earlier. The individual $[\text{HbR}]$, $[\text{HbO}_2]$ and $[\text{HbT}]$ time courses from five rats were

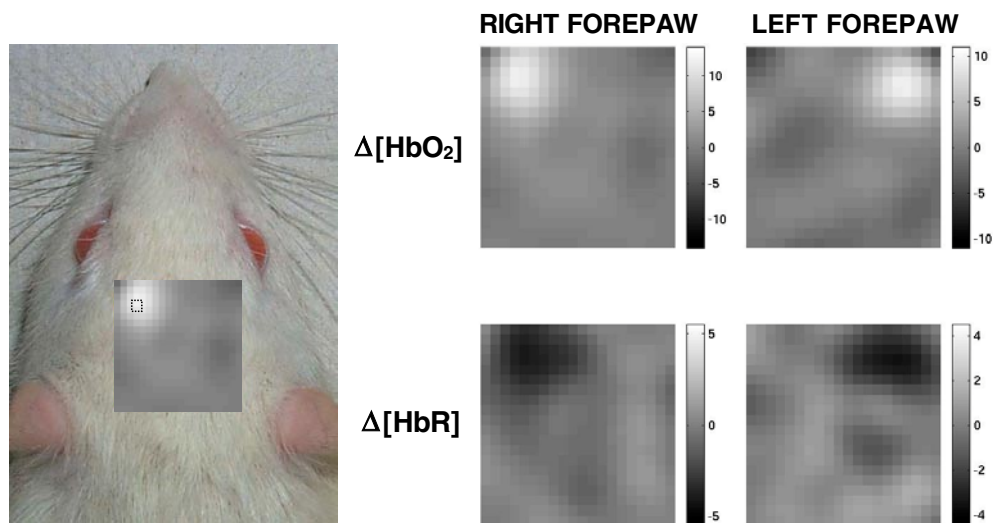


Figure 2. Spatially resolved DOT images from a single rat showing contralateral activation of the somatosensory cortex. The dashed square indicates the pixel showing maximal activation, from which the time courses would be obtained.

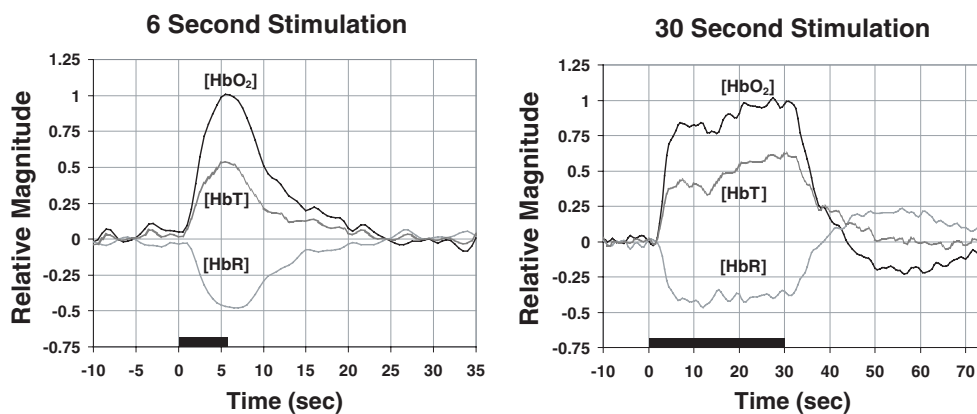


Figure 3. DOT time courses at 3 Hz stimulation for both 6 and 30 s, showing the relative magnitudes of [HbR], [HbO₂] and [HbT]. The transient increase in [HbO₂] is greater than the corresponding decrease in [HbR], leading to a net increase in [HbT] following stimulation. The black bars represent the duration of stimulation, and uncertainty is shown by the error bars in figure 4 which presents this data in greater detail.

first normalized and then group-averaged, using the stimulus onset time for synchronization. A plot of the relative magnitudes of these time courses is shown in figure 3.

Shown for comparison are CBV and BOLD results from fMRI data collected under similar conditions. Figure 4 shows the group-averaged temporal evolution of DOT [HbR] and [HbO₂] plotted with the fMRI BOLD signal, and DOT [HbT] plotted with the fMRI cerebral plasma volume (CPV). Since the differences in the fMRI datasets collected at 2.0 T and 4.7 T were not statistically significant, the curves for all but the 6 s CPV dataset (which was measured at

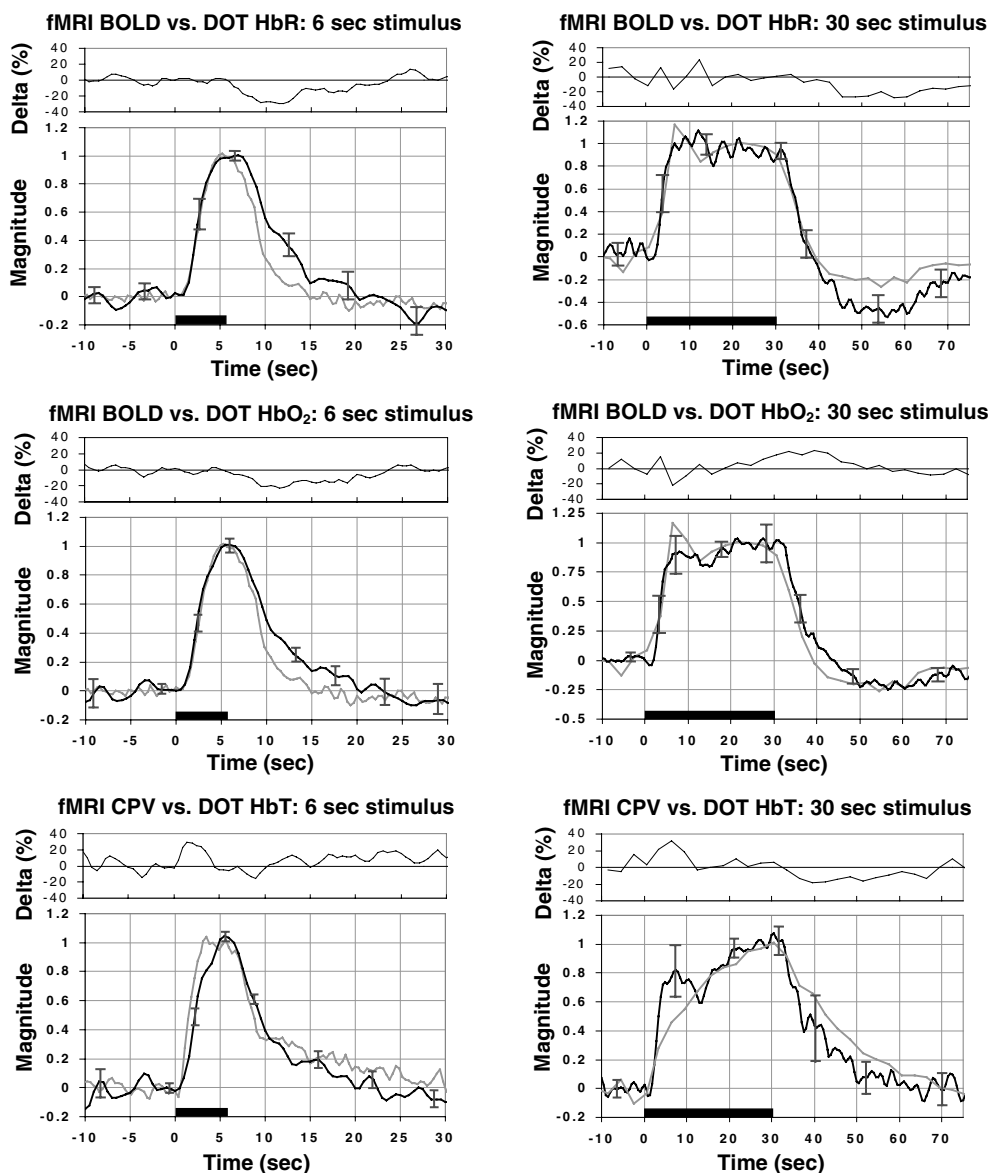


Figure 4. The temporal evolution of cerebral blood volume and haemoglobin concentration, as measured with fMRI (grey curves) and DOT (black curves) at a forepaw stimulus current of 2 mA. Error bars are shown for the DOT data, and fMRI/DOT delta versus time curves are shown above each plot. Uncertainty in the fMRI data is comparable (Mandeville *et al* 1999a, Mandeville and Marota 1999). The fMRI curves (except for the 6 s CPV dataset, measured at 2.0 T only) show the average of data collected at both 2.0 T and 4.7 T.

2.0 T only) show the averaged results of the datasets collected at both 2.0 T and 4.7 T field strengths (Mandeville *et al* 1999a).

The plots in figure 5 show the effect of several stimulus parameters on the DOT [HbO₂] response. Since the [HbO₂] and [HbR] responses were similar in shape (albeit opposite in

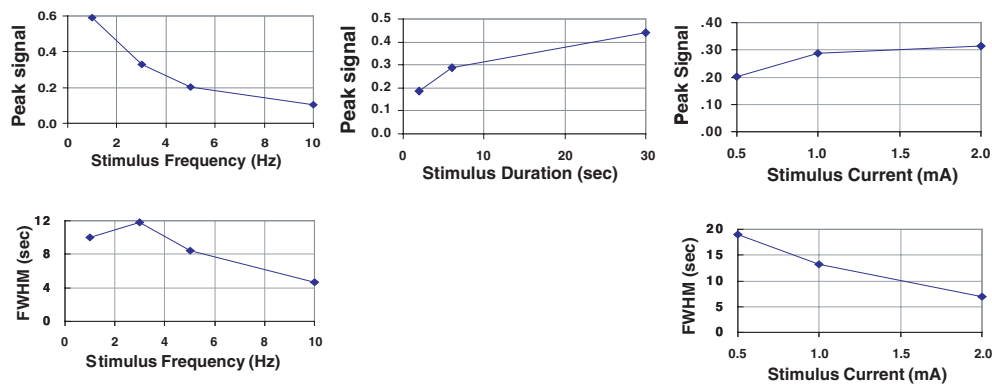


Figure 5. [HbO₂] peak signal magnitude and FWHM (in arbitrary units) versus stimulus frequency, current and duration. Unless otherwise noted, the nominal test conditions were: $F_{\text{stim}} = 3$ Hz, $I_{\text{stim}} = 1.0$ mA, $T_{\text{stim}} = 6$ s. See text for details.

direction), only the larger [HbO₂] response is shown. Each plot consists of the contiguously collected data from two rats.

4. Discussion

DOT and fMRI provide similar measures of hemodynamic activity. Both employ haemoglobin as an endogenous contrast agent; however, there are significant differences in how it is actually detected. They also differ in how they measure cerebral blood volume. Although the detection mechanisms of DOT and fMRI differ and sensitivity varies with vessel diameter for both methods, they may still provide similar temporal information if their vascular weighting functions are comparable (Menon *et al* 1995a).

4.1. Vascular sensitivity of fMRI and DOT

Because [Hbr] is a paramagnetic contrast agent for MRI, BOLD fMRI detects local magnetic field perturbations produced by absolute changes in [Hbr] within each voxel. Since HbO₂ is diamagnetic like surrounding tissue, it has minimal influence on proton precession and thus cannot be measured with fMRI. Cerebral plasma volume was measured with the aid of MION, an exogenous superparamagnetic contrast agent, yielding a signal proportional to the change in total plasma volume fraction within each voxel (Mandeville *et al* 1998). DOT detects changes in [Hbr] and [HbO₂] by measuring their effect on the optical absorption properties within the tissue. Measurements at multiple source wavelengths allow the relative contributions of each component to be calculated independently. Thus DOT can measure changes in [Hbr], [HbO₂] and [HbT] simultaneously, without the need for exogenous contrast agents. The DOT voxel locations were chosen for analysis based upon the maximum HbT response. HbT provided better spatial localization than HbR because the locus of the HbR signal shifted with time as HbR-rich blood presumably traversed the local draining veins.

DOT is subject to its own concerns and limitations. As the image reconstruction process is ill-posed, it can lead to errors in the hemodynamic characterization. In an effort to reduce both spatial and [Hb] estimation errors, we chose optical sources centred at 690 nm and 830 nm, since it is believed that a source wavelength of 690 nm is preferable to 780 nm

when paired with an 830 nm source for DOT (Strangman *et al* 2003, Yamashita *et al* 2001). Also, features with high absorbance, such as large blood vessels, can absorb nearly all of the local incident flux, thus reducing DOT signal sensitivity in these areas. Thus, most DOT measurements are uniformly sensitive to vessels smaller than the optical absorption length, with sensitivity progressively decreasing for larger vessels (Liu *et al* 1995).

4.2. Comparison of the hemodynamic response functions

The data in figure 3 show the typical hemodynamic response pattern, with an event-related increase in $[\text{HbO}_2]$ accompanied by a smaller decrease in $[\text{HbR}]$. The hemodynamic responses following both 6 and 30 s stimulation were delayed approximately 2 s from stimulus onset, which is consistent with similar human studies. Following stimulus onset, the $[\text{HbO}_2]$ and $[\text{HbT}]$ both peaked at ~ 5 s and the $[\text{HbR}]$ peaked at ~ 7 s, which has also been seen in humans (Boas *et al* 2003, Jadzewsky *et al* 2003). Unlike those studies, which observed a ~ 1 s difference between the onset of the HbO_2 and HbR responses, the rise in $[\text{HbO}_2]$ nearly coincided with the fall in $[\text{HbR}]$ in both the 6 and 30 s data. This might be due to the shorter cerebral mean transit time in rats as compared to humans. In whisker barrel cortex, some have seen similar results (Jones *et al* 2002), while others observed the change in $[\text{HbO}_2]$ leading $[\text{HbR}]$ by about 1 s (Kohl *et al* 2000).

For the 30 s stimulus, the data show a post-stimulus overshoot in $[\text{HbR}]$ and undershoot in $[\text{HbO}_2]$, both of which slowly returned from their peak values to baseline after ~ 30 s. The $[\text{HbT}]$ did not exhibit any undershoot, however, and returned to baseline within ~ 20 s of cessation of stimulation. The hemodynamics following the 6 s stimulus did not exhibit any under- or overshoot, which is presumably due to the brevity of the stimulus in relation to the length of time required to achieve vascular delayed compliance (Mandeville *et al* 1999b).

Although there is an overall scale factor between DOT and fMRI data, signals normalized to the main response can be compared for similarity in the post-stimulus region. The DOT $[\text{HbT}]$ time courses followed the 6 and 30 s fMRI CPV time courses reasonably well, showing similar profiles in both cases. In principle, both modalities should exhibit near linear proportionality to changes in the blood volume fraction, provided that the hematocrit within the region of activation remains constant during the measurement (Mandeville and Marota 1999, Cheng and Boas 1999). However, it is possible that blood plasma volume (and thus hematocrit) may vary following cerebral activation, though this has not yet been confirmed (Jones *et al* 2002). If so, then this could introduce nonlinearities in both the DOT $[\text{HbT}]$ and fMRI CPV responses. The DOT $[\text{HbT}]$ response showed a rapid initial rise to a transient peak about 5 s after stimulus onset, followed by a later slow rise. Using rapid sampling, fMRI data also showed this multi-phasic response in blood plasma volume (Mandeville *et al* 1999b). Although the transient peak observed in the DOT $[\text{HbT}]$ data was not present in the averaged fMRI data, it was observed in individual rats. Also interesting is a similar transient peak in estimated CMRO_2 following whisker barrel stimulation at 1.6 mA (Jones *et al* 2002).

The DOT $[\text{HbR}]$ and $[\text{HbO}_2]$ 30 s time courses both tracked the fMRI BOLD time course within the stimulus region, but their behaviour in the post-stimulus region differed. $[\text{HbR}]$ showed a more pronounced undershoot than either $[\text{HbO}_2]$ or BOLD, although its contour (i.e. the shape of the curve) matched the BOLD signal very closely. The $[\text{HbO}_2]$ tracked the BOLD signal better in magnitude than did $[\text{HbR}]$, but the contours of the two time courses appeared to differ. Although $[\text{HbR}]$ and BOLD signal in the post-stimulus region cannot be shown to differ statistically given the variability between animals, as reflected by the error bars in figure 4, there are several potential sources of discrepancy between the two modalities. The most likely of these are the following.

1. BOLD fMRI includes contributions from intravascular blood water, as well as extravascular water that is influenced by gradients extending from the blood vessels. The latter effect is expected to be roughly linear with [HbR], while the former effect is most pronounced at low fields (Boxerman *et al* 1995) and diminishes at higher field strengths (Menon *et al* 1995b). Elevated blood volume ([HbT] and CPV) in the post-stimulus region should produce a negative effect on both HbR and extravascular BOLD signal, whereas elevated blood water will increase intravascular BOLD signal at low fields due to the longer T₂ of blood relative to parenchyma. For this reason, high-field BOLD signal should more closely reflect [HbR] in the post-stimulus region if the source of the post-stimulus undershoot is elevated CBV. In fact, the BOLD post-stimulus undershoot in the 4.7 T data was observed to be larger than that in the 2 T data (Mandeville *et al* 1999a), consistent with this explanation.
2. DOT and fMRI undoubtedly sample the activated volume with different sensitivity profiles, particularly with respect to depth from the cortical surface. Since the temporal evolution of the cerebral hemodynamic response is influenced by the arterial, capillary and venous compartments, fMRI and DOT are likely governed by different weightings of these three vascular compartments.

4.3. Significance of [HbO₂] undershoot

Based upon the fMRI measurements in this model (Mandeville *et al* 1998, 1999a), the mechanism of the BOLD post-stimulus undershoot has been suggested to be a temporal mismatch between blood flow and volume. In this optical imaging study, [HbO₂] adds information that is not directly available from fMRI. Significantly, we note that the temporal profile of [HbO₂] shows a post-stimulus undershoot. There are two possible explanations for this. One explanation is that arterial blood volume undershoots the baseline following stimulation, which would contribute to [HbO₂] only. Since CBF has been observed to undershoot following stimulation in some models (Hoge *et al* 1999), this possibility cannot be discounted.

However, perhaps a more parsimonious explanation is that the transient post-stimulus features of [HbR], [HbO₂], and [HbT] are temporally similar because they derive from a common physiological source. It has been postulated that blood volume is elevated only in the venous compartment following stimulation (Mandeville *et al* 1999b). However, if the capillary compartment shows the same temporal response, this could consistently explain all the optical data. In a diffusion-limited model of oxygen delivery from the blood to brain tissue (Buxton and Frank 1997), elevated capillary blood volume provides a mechanism to increase oxygen delivery even if CBF has returned to baseline. Thus, [HbO₂] would show a post-stimulus undershoot, [HbT] would show a slow post-stimulus decay due to a slow response of both capillary and venous CBV, and the mechanism of the [HbR] overshoot would be attributed to both elevated CBV and an increased rate of oxygen utilization (CMRO₂).

4.4. Dependence on stimulation parameters

In order to investigate the robustness of the forepaw stimulation paradigm and to illustrate the utility of DOT for functional imaging studies, the hemodynamic effects of various parameters were explored. Figure 5 shows the FWHM and peak signal magnitude of [HbO₂] (in arbitrary units) versus stimulus frequency, current and duration. Since the relative magnitudes of [HbO₂] and [HbR] responses were qualitatively similar (albeit opposite in direction), only the [HbO₂] response is shown. Each dataset was collected from only two rats, and should be considered as qualitative observations.

The $[\text{HbO}_2]$ signal magnitude increased sublinearly (i.e. compressed) with increasing stimulus current. If correct, this implies that a saturation in neural activation occurs at a stimulus current near 2 mA. In a plot presented by Spenger *et al* (2000), the majority of their data shows a similar plateau in response amplitude at ~ 1.5 mA. The FWHM of the hemodynamic response decreased significantly with increasing stimulus current; however, the onset delay remained constant. The signal magnitude and FWHM both grew sublinearly with increasing stimulus duration out to 30 s.

Signal magnitude decreased in approximate inverse proportion to stimulus frequency. This trend was also observed by Gyngell *et al* and Brinker *et al*, who both noted a decrease in $T2^*$ fMRI contrast with increasing stimulus frequency, and attributed it to a progressive reduction in the neuronal recovery time (Gyngell *et al* 1996, Brinker *et al* 1999). The FWHM appeared to peak at 3 Hz and then decreased in inverse proportion to stimulus frequency. This could result from frequency-sensitive activation of different neural pathways within the cortex, each of which may elicit different hemodynamic responses. Similar research on rat whisker barrel cortex has revealed frequency-selective or 'tuned' neural responsivity versus stimulus frequency, which appeared as a variation in the spatial extent of activation (Moore *et al* 1999). It is conceivable that a similar frequency-dependent neural activation also occurs during forepaw stimulation, and this might account for our observations. This could also result from habituation, which would cause progressive neuronal attenuation with increasing frequency.

Signal amplitude was also observed to vary with electrode placement (data not shown). Although total stimulus current is easy to quantify, the actual current distribution within the forepaw itself is not easily measured. In future experiments, this aspect will need to be addressed more carefully, perhaps by using monitor electrodes to directly assess the degree of neural activation.

5. Conclusions

Both DOT $[\text{HbR}]$ and $[\text{HbO}_2]$ compared well to fMRI BOLD during stimulation but their profiles differed in the post-stimulus region, which suggests that different hemodynamic mechanisms might be responsible for the post-stimulus responses of the $[\text{HbR}]$ and $[\text{HbO}_2]$ signals. The DOT $[\text{HbT}]$ time courses followed the 6 and 30 s fMRI CPV time courses reasonably well. The similarity of the DOT and MRI hemodynamic measures suggests that the vascular sensitivity of the two methods is qualitatively similar, but not identical.

Acknowledgments

The authors acknowledge financial support from NIH R29-NS38842, NIH K25-NS44339 and P41-RR14075.

References

- Ances B M, Wilson D F, Greenberg J H and Detre J A 2001 Dynamic changes in cerebral blood flow, O_2 tension, and calculated cerebral metabolic rate of O_2 during functional activation using oxygen phosphorescence quenching *J. Cereb. Blood Flow Metab.* **21** 511–6
- Arridge S R 1999 Optical tomography in medical imaging *Inverse Problems* **15** R41–93
- Arthurs O J, Williams E J, Carpenter T A, Pickard J D and Boniface S J 2000 Linear coupling between functional magnetic resonance imaging and evoked potential amplitude in human somatosensory cortex *Neuroscience* **101** 803–6

- Benaron D A, Hintz S R, Villringer A, Boas D, Kleinschmidt A, Frahm J, Hirth C, Obrig H, van Houten J C, Kermit E L, Cheong W F and Stevenson D K 2000 Noninvasive functional imaging of human brain using light *J. Cereb. Blood Flow Metab.* **20** 469–77
- Berns G S 1999 Functional neuroimaging *Life Sci.* **65** 2531–40
- Boas D A, Franceschini M A, Dunn A K and Strangman G A 2002 *In Vivo Optical Imaging of Brain Function* ed Frostig R D (Boca Raton: CRC Press) pp 193–221
- Boas D A, Gaudette T, Strangman G, Cheng X, Marota J J and Mandeville J B 2001 The accuracy of near infrared spectroscopy and imaging during focal changes in cerebral hemodynamics *Neuroimage* **13** 76–90
- Boas D A, Jaszewski G, Culver J, Poldrack R A, Mandeville J and Strangman G 2003 Estimation of the cerebral metabolic rate of oxygen with near infrared spectroscopy *Phys. Med. Biol.* submitted
- Boxerman J L, Bandettini P A, Kwong K K, Baker J R, Davis T L, Rosen B R and Weisskoff R M 1995 The intravascular contribution to fMRI signal change: Monte Carlo modeling and diffusion-weighted studies *in vivo Magn. Reson. Med.* **34** 4–10
- Brinker G, Bock C, Busch E, Krep H, Hossmann K A and Hoehn-Berlage M 1999 Simultaneous recording of evoked potentials and T2*-weighted MR images during somatosensory stimulation of rat *Magn. Reson. Med.* **41** 469–73
- Buxton R B and Frank L R 1997 A model for the coupling between cerebral blood flow and oxygen metabolism during neural stimulation *J. Cereb. Blood Flow Metab.* **17** 64–72
- Cheng X and Boas D A 1999 Systematic diffuse optical image errors resulting from uncertainty in the background optical properties *Opt. Express.* **4** 299–307
- Cope M 1991 *The Development of a Near-Infrared Spectroscopy System and its Application for Noninvasive Monitoring of Cerebral Blood and Tissue Oxygenation in the Newborn Infant* (London: University College London)
- Cope M and Delpy D T 1988 System for long-term measurement of cerebral blood flow and tissue oxygenation on newborn infants by infra-red transillumination *Med. Biol. Eng. Comput.* **26** 289–94
- Culver J P, Choe R, Holboke M R, Zubkov L, Durduran T, Slemp A, Ntziachristos V, Chance B and Yodh A G 2002 Three-dimensional diffuse optical tomography in the parallel plane transmission geometry: evaluation of a hybrid frequency domain/continuous wave clinical system for breast imaging
- Dale A M and Halgren E 2001 Spatiotemporal mapping of brain activity by integration of multiple imaging modalities *Curr. Opin. Neurobiol.* **11** 202–8
- Gaudette R J 2000 A comparison study of linear reconstruction techniques for diffuse optical tomographic imaging of absorption coefficient *Phys. Med. Biol.* **45** 1051–70
- Gyngell M L, Bock C, Schmitz B, Hoehn-Berlage M and Hossmann K A 1996 Variation of functional MRI signal in response to frequency of somatosensory stimulation in alpha-chloralose anesthetized rats *Magn. Reson. Med.* **36** 13–5
- Habel U, Posse S and Schneider F 2002 Fundamentals of functional magnetic resonance imaging in clinical psychology and psychiatry *Fortschr. Neurol. Psychiatr.* **70** 61–70
- Hansen P C 1998 *Rank-Deficient and Discrete Ill-Posed Problems: Numerical Aspects of Linear Inversion* (Philadelphia: SIAM)
- Hintz S R, Benaron D A, Siegel A M, Zourabian A, Stevenson D K and Boas D A 2001 Bedside functional imaging of the premature infant brain during passive motor activation *J. Perinat. Med.* **29** 335–43
- Hoge R D, Atkinson J, Gill B, Crelier G R, Marrett S and Pike G B 1999 Stimulus-dependent BOLD and perfusion dynamics in human V1 *Neuroimage* **9** 573–85
- Jadzewsky G, Strangman G, Wagner J, Kwong K K, Poldrack R A and Boas D A 2003 Differences in the early hemodynamic response to event-related motor and visual paradigms as measured by near infrared spectroscopy *NeuroImage* submitted
- Jones M, Berwick J and Mayhew J 2002 Changes in blood flow, oxygenation, and volume following extended stimulation of rodent barrel cortex *NeuroImage* **15** 474–87
- Kienle A and Patterson M S 1997 Improved solutions of the steady-state and the time-resolved diffusion equations for reflectance from a semi-infinite turbid medium *J. Opt. Soc. Am. A.* **14** 246–54
- Kleinschmidt A, Obrig H, Requardt M, Merboldt K D, Dirnagl U, Villringer A and Frahm J 1996 Simultaneous recording of cerebral blood oxygenation changes during human brain activation by magnetic resonance imaging and near-infrared spectroscopy *J. Cereb. Blood Flow Metab.* **16** 817–26
- Kohl M, Lindauer U, Royl G, Kuhl M, Gold L, Villringer A and Dirnagl U 2000 Physical model for the spectroscopic analysis of cortical intrinsic optical signals *Phys. Med. Biol.* **45** 3749–64
- Liu H, Chance B, Hielscher A H, Jacques S L and Tittel F K 1995 Influence of blood vessels on the measurement of hemoglobin oxygenation as determined by time-resolved reflectance spectroscopy *Med. Phys.* **22** 1209–17
- Mandeville J B and Marota J J 1999 Vascular filters of functional MRI: spatial localization using BOLD and CBV contrast *Magn. Reson. Med.* **42** 591–8

- Mandeville J B, Marota J J, Ayata C, Moskowitz M A, Weisskoff R M and Rosen B R 1999a MRI measurement of the temporal evolution of relative CMRO(2) during rat forepaw stimulation *Magn. Reson. Med.* **42** 944–51
- Mandeville J B, Marota J J, Ayata C, Zaharchuk G, Moskowitz M A, Rosen B R and Weisskoff R M 1999b Evidence of a cerebrovascular postarteriole windkessel with delayed compliance *J. Cereb. Blood Flow Metab.* **19** 679–89
- Mandeville J B, Marota J J, Kosofsky B E, Keltner J R, Weissleder R, Rosen B R and Weisskoff R M 1998 Dynamic functional imaging of relative cerebral blood volume during rat forepaw stimulation *Magn. Reson. Med.* **39** 615–24
- Marota J J, Ayata C, Moskowitz M A, Weisskoff R M, Rosen B R and Mandeville J B 1999 Investigation of the early response to rat forepaw stimulation *Magn. Reson. Med.* **41** 247–52
- Menon R S, Kim S G, Hu X, Ogawa S and Ugurbil K 1995a *Diffusion and Perfusion Magnetic Resonance Imaging* ed D Le Bihan (New York: Raven Press) pp 327–49
- Menon R S, Ogawa S, Hu X, Strupp J P, Anderson P and Ugurbil K 1995b BOLD based functional MRI at 4 Tesla includes a capillary bed contribution: echo-planar imaging correlates with previous optical imaging using intrinsic signals *Magn. Reson. Med.* **33** 453–9
- Moore C I, Nelson S B and Sur M 1999 Dynamics of neuronal processing in rat somatosensory cortex *Trends Neurosci.* **22** 513–20
- Silva A C, Lee S P, Yang G, Iadecola C and Kim S G 1999 Simultaneous blood oxygenation level-dependent and cerebral blood flow functional magnetic resonance imaging during forepaw stimulation in the rat *J. Cereb. Blood Flow Metab.* **19** 871–9
- Spenger C, Josephson A, Klason T, Hoehn M, Schwindt W, Ingvar M and Olson L 2000 Functional MRI at 4.7 tesla of the rat brain during electric stimulation of forepaw, hindpaw, or tail in single- and multislice experiments *Exp. Neurol.* **166** 246–53
- Strangman G, Culver J P, Thompson J H and Boas D A 2002 A quantitative comparison of simultaneous BOLD fMRI and NIRS recordings during functional brain activation *Neuroimage* **17** 719–31
- Strangman G, Franceschini M A and Boas D A 2003 Factors affecting the accuracy of near-infrared spectroscopy (NIRS) data analysis for focal changes in hemodynamics *NeuroImage* at press
- Toronov V, Webb A, Choi J H, Wolf M, Michalos A, Gratton E and Hueber D 2001 Investigation of human brain hemodynamics by simultaneous near-infrared spectroscopy and functional magnetic resonance imaging *Med. Phys.* **28** 521–7
- Villringer A and Chance B 1997 Non-invasive optical spectroscopy and imaging of human brain function *Trends Neurosci.* **20** 435–42
- Villringer A and Dirnagl U 1995 Coupling of brain activity and cerebral blood flow: basis of functional neuroimaging *Cerebrovasc. Brain. Metab. Rev.* **7** 240–76
- Yamashita Y, Maki A and Koizumi H 2001 Wavelength dependence of the precision of noninvasive optical measurement of oxy-, deoxy-, and total-hemoglobin concentration *Med. Phys.* **28** 1108–14